Proceedings of 2001 Korea-Japan Joint Seminar
on Particle Image Velocimetry
Seoul National Univ., Dec. 3 - 4

Dual-plane Stereoscopic PIV Measurement on the Lobed Jet Mixing Flow

Tetsuo SAGA, Toshio KOBAYASHI

Institute of Industrial Science, The University of Tokyo
4-6-1 Komaba Meguro-Ku Tokyo 153-8505

Abstract In a continuing effect to study the mixing enhancement by large-scale streamwise vortices in lobed mixing flows, an advanced PIV system named as dual-plane stereoscopic PIV system was used in the present study to conduct simultaneous vorticity (all three components) measurement of an air jet exhausted from a lobed nozzle. Unlike "classical" 2-D PIV system or conventional "single-plane" stereoscopic PIV system, the dual-plane stereoscopic PIV system used in the present study can obtain the flow velocity (all three components) fields at two spatially separated planes simultaneously. Therefore, it can provide the distributions of all the three components of vorticity vectors instantaneously and simultaneously. The evolution and interaction characteristics of the large-scale streamwise vortices and azimuthal Kelvin-Helmholtz vortices in the lobed jet mixing flow were revealed instantaneously and quantitatively from the measurement results of the dual-plane stereoscopic PIV system. The characteristics of the mixing process in the lobed jet mixing flow were analyzed based on the simultaneous measurement results of the steamwise vorticity and azimuthal Kelvin-Helmholtz vorticity distributions.

1. Introduction

Lobed mixers/nozzles, which are essentially splitter plates with corrugated trailing edges, are fluid mechanic devices used to augment mixing in a variety of applications. Such devices have been applied widely in turbofan engine exhausts and ejectors to reduce take-off jet noise and Specific Fuel Consumption (SFC) (Kuchar et al. 1980, Presz et al. 1994, Hu et al. 1999). More recently, lobed mixers/nozzles have also emerged as an attractive approach for enhancing mixing between fuel and air in combustion chambers to improve the efficiency of combustion and reduce the formation of pollutants (Smith et al.1997).

Due to the excellent mixing enhancement performance and widely potential applications of the lobed mixers/nozzles, extensively studies about the mechanism by which lobed nozzles/mixers substantially enhance the mixing have been conducted. Based on pressure, temperature, and velocity measurements of the flow field downstream an axisymetric lobed nozzle, Paterson (1984) revealed the existence of large-scale streamwise vortices due to the secondary flow in the lobed mixing flow induced by the special geometry of the lobed nozzle. Horseshoe vortices with smaller scale were also found to exist at the lobe troughs. Although the contribution of these vortices to the overall mixing process was not clear, the large-scale streamwise vortices were believed to be responsible for the enhanced mixing because of their much greater size. Werle et al. (1987) and Eckerle et al. (1992) found that the large-scale streamwise vortices in a lobed mixing flow follow a three-step process by which the streamwise vortices form, intensify, and then break down. They also found that the breakdown of the vortices was accompanied by a significant increase in turbulent mixing. Elliott et al. (1992) suggested that there are three primary contributors to the mixing processes in lobed mixing flows. The first is the azimuthal vortices, which occur in any free

shear layers due to the Kelvin-Helmholtz instability. The secondary is the increased interfacial contact area due to the convoluted trailing edge of the lobed mixer. The last element is the streamwise vortices produced by the special geometry of the lobed mixer. Based on the pulsed-laser sheet flow visualization with smoke and three-dimensional velocity measurements with Hot Film Anemometer, McCormick and Bennette (1994) suggested that it is the interaction of the azimuthal Kelvin-Helmholtz vortices with the streamwise vortices produces the high levels of mixing. As the azimuthal Kelvin- Helmholtz vortices shed from the trailing edge of lobed mixers, the streamwise vortices deform them until they are eventually pinched off and subsequently broken down. Turbulence measurements showed the regions of high-turbulence kinetic energy that were consistent with the flow visualization of the pinch-off effect.

2. Experimental Setup

2.1 Dual-plane stereoscopic PIV system

It is well known that particle scattering can be either Mie scattering or Rayleigh scattering depending on the relative diameter of the particle compared with the wavelength (λ) of the incident light. According to McCartney (1976), Mie scattering is generally defined as scattering from particles which is greater than 1/10 of the incident light wavelength (λ) and Rayleigh scattering is defined as scattering form particle with diameters less than $1/10\lambda$.

In the Mie scattering regime, the scattering will have a dominant forward direction, and nonuniform "lobed" scattering towards the sides. The scattering distributions will depend upon the particle size, incident light wavelength and polarization. It should be mentioned that the polarization direction is conservative in the Mie scattering regime if the incident light is linearly polarized, and the Mie scattering pattern tends to go nearly to zero (due to depolarization) in the direction normal to the incident polarization direction (Elliott and Beutner, 1999). As the same as Keahler and Kompenhance (1999), the dual-plane stereoscopic PIV system used in the present study utilizes the polarization direction conservation characteristics of the Mie scattering to separate the light scattering from the two illuminating laser sheets to achieve simultaneous stereoscopic PIV measurements at two spatially separated planes.

Figure 1 shows the schematic set-up of the dual-plane stereoscopic PIV system used in the present study. Two sets of widely used double-plused Nd:YAG lasers (New Wave, 50mJ/pulse) with additional optics (half wave plate, mirrors, polarizer and cylinder lens) were used to set up the illumination system of the dual-plane stereoscopic PIV system. The P-polarized laser beams from the double-pulsed Nd:YAG laser set A were turn into S-polarized light by passing a half wave ($\lambda/2$)plate before they are combined with the P-polarized laser beams from the double-pulsed Nd:YAG laser set B. The P-polarized laser beams from the laser set B transmit through the Polarizer cube, while the S-polarized light from the double-pulsed Nd:YAG laser set A are reflected by the Polarizer cube. By adjusting the angular and/or the location of the mirror #1, the laser beams from the laser set A and laser set B can be overlapped or not. Passing through the cylindrical lens and reflected by mirror #2, the laser beams are expanded into two paralleling laser sheets with orthogonal linear polarization to illuminate the studied flow field at two spatially separated planes. In the present study, the thickness of the illuminating laser sheets is about 2.0mm, and the gap between the centers of the two illuminated planes is adjusted as 2.0 mm. For capturing the stereoscopic PIV images simultaneously at two measurement planes illuminated by the two laser sheets with orthogonal linear polarization, two pairs of high-resolution cross-correlation CCD cameras (1K by 1K, TSI PIVCAM 10-30) were used to do stereoscopic PIV image recording. The two pairs of the high-resolution CCD cameras were settled on an optical table with a pair of polarizing beam splitter cubes and two high reflectivity mirrors installed in front of the cameras to

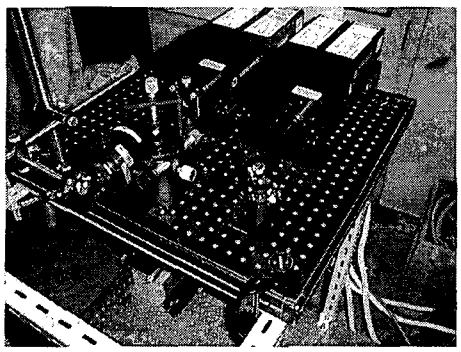

Illumination System

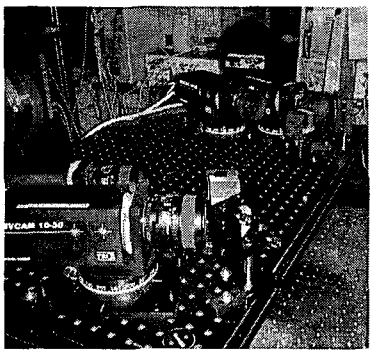

Photographic System

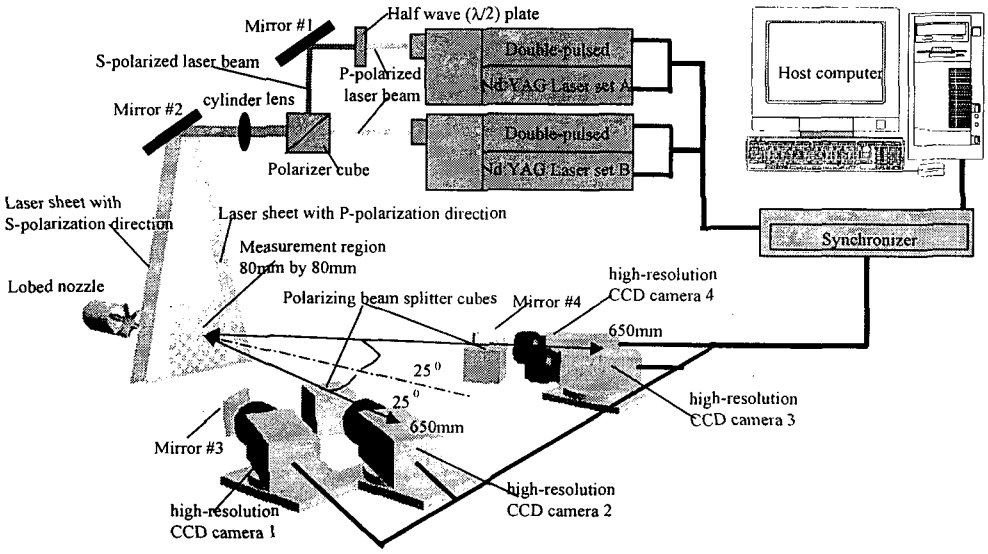

Fig. 1. The schematic set-up of the dual-plane stereoscopic PIV system

separate the scattered light from the two illuminating laser sheets with orthogonal linear polarization. The illuminating laser sheets with orthogonal linear polarization are scattered by the tracer particles seeded in the objective fluid flow. Due to the polarization direction conservation characteristics of the Mie scattering mentioned above, the scattered light from the P-polarized laser sheet will keep the P-polarization direction and pass straight through the polarizing beam-splitter cubes and is detected by cameras 2 and 3. The scattered light from the S-polarized laser sheet will still be S-polarization and emerge from the polarizing beam splitter cubes at the right angles to the incident direction. Reflected by the two high reflectivity mirrors (mirror #3 and #4), the scattered S-polarized light is detected by the cameras 1 and 4.

In order to maximized the size of measurement window, the two pairs of high-resolution CCD cameras were arranged in an angular displacement configuration. With the installation of tilt-axis mounts, the lenses and camera bodies were adjusted to satisfy Scheimpflug condition (Prasad and Jensen, 1995)to obtain focused particle images everywhere in the image recording planes. In the present study, the distance between the illuminating laser sheet and image recording planes of the CCD cameras is about 650mm, and the angle between the optical axis of the two cameras is about 50^0. For such arrangement, the size of the stereoscopic PIV measurement window is about 80mm by 80mm.

The CCD cameras and double-pulsed Nd:YAG laser sets were connected to a workstation (host computer) via a synchronizer (TSI LaserPulse synchronizer), which controlled the timing of the laser sheet illumination and the CCD camera data acquisition. In the present study, the time interval between the two pulsed illuminations was set as 30 μ s.

A general three-dimensional (3-D) in-situ calibration procedure was conducted in the present study to obtain the mapping functions between the image planes and object planes (Soloff et al. 1997). A target plate (100mm by 100mm) with 100μm diameter dots spaced at interval of 2.5 mm was used for the in-situ calibration. The front surface of the target plate was aligned with the center of the laser sheet and then calibration images were captured at three locations across the depth of the laser sheets. The space interval between these locations was 0.5mm for the present study. The mapping function used in the present study was taken to be a multi-dimensional polynomial, which is fourth order for the directions (X and Y directions) paralleling the laser sheet plane and second order for the direction (Z direction) normal to the laser sheet plane. The coefficients of the multi-dimensional polynomial were determined from the calibration images by using least square method.

It should be mentioned that the present dual-plane stereoscopic PIV system uses the same polarization direction separation method as Kaehler and Kompenhans (1999) to do the scattered light separation. In contrast to the 2-D calibration method used by Kaehler and Kompenhans (1999), the general 3-D in-situ calibration procedure (Soloff et al. 1997) was used in the present study to determine the relationships between the three-dimensional objective fields and the two-dimensional image planes. For the 2-D calibration used by Kaehler and Kompenhans (1999), mapping functions are sought only to relate each two-dimensional image planes to the two-dimensional objective planes. It should be noted that these quantities pertaining to the recording geometry may be difficult to measure accurately and may introduce errors. Furthermore, if recording is accomplished through a liquid-air interface, the reconstruction equations will need to be modified to account for the refraction at the interface (Prasad, 2000).The general 3-D in-situ calibration method used in the present study can incorporate all the parameters of system geometry and optical arrangement automatically and do not need any explicit input for both position mapping and velocity three-component reconstruction.

2.2 Lobed Jet Mixing Flow and Experimental Apparatus

Figure 2(a) shows the geometry parameters of the lobed nozzle used in the present study. The lobed nozzle has six lobes. The width of each lobes is 6mm and the height of each lobe is 15mm (H=15mm). The inner and outer penetration angles of the lobed structures are about 22^0 and 14^0 respectively. The diameters of the lobed nozzles is D=40mm.

Figure 2(b) shows the jet flow experimental rig used in the present study. The air jet was supplied by a centrifugal compressor. A cylindrical plenum chamber with honeycomb structures in it was used for settling the airflow. Through a convergent connection (contraction ratio is about 50:1), the airflow is exhausted from the test nozzle. All the jet supply apparatus were installed on a two-dimensional translation mechanism so that the distance between the exit plane of the lobed nozzle and the illuminating laser sheets can be changed by operating the two-dimensional translation mechanism. The illumination system and image recording system are fixed during the experiment, the measurements for the different cross planes of the lobed jet mixing flow were achieved by changing the positions of the lobed nozzle. Therefore, all the measurements at the different cross-planes of the lobed jet mixing flow can be conducted by doing the in-situ calibration procedure only once.

The velocity of the air jet exhausting from the test nozzle is adjustable. In the present study, the jet velocity (U_0) was set at about 20m/s. The Reynolds number of the jet flow, based on the lobed nozzle diameter (D) and the jet velocity is about 60,000.

A seeding generator, which is composed by an air compressor and several Laskin nozzles (Melling, 1997), was used to generate 1~5μm DEHS (Di-2-EthlHexyl-Sebact) droplets as tracer particles in the jet mixing flow. The seeding DEHS droplet flow from the seeding generator are divided into two streams; one is used to seed the core jet flow and another for the ambient air seeding.

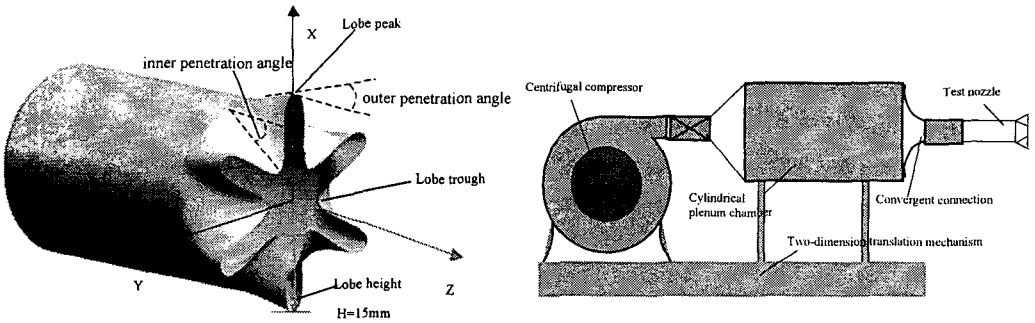

Fig. 2, The test lobed nozzle and experimental rig used in the present study

3. Experimental results and discussions

Figure 3 gives a pair of typical instantaneous measurement results obtained simultaneously by the dual-plane stereoscopic PIV system in two parallel cross planes (Z=10mm and Z=12mm) near the exit of lobed nozzle. 32 pixel by 32 pixel windows were used for the correlation operation, the spatial resolution of the present stereoscopic PIV measurement is expected to be about 2mm×2mm×2mm. Since the characteristics of the mixing process in the lobed jet mixing flow revealed from the velocity distributions has been discussed extensively in the earlier work of the authors (Hu et al., 2000a,b and 2001a), the majority of the results and discussions given in the present paper will focus on the evolution and interaction characteristics of various vortical and turbulent structures in the lobed jet mixing flow revealed from the simultaneous measurement results of the streamwise vorticity and azimuthal vorticity fields.

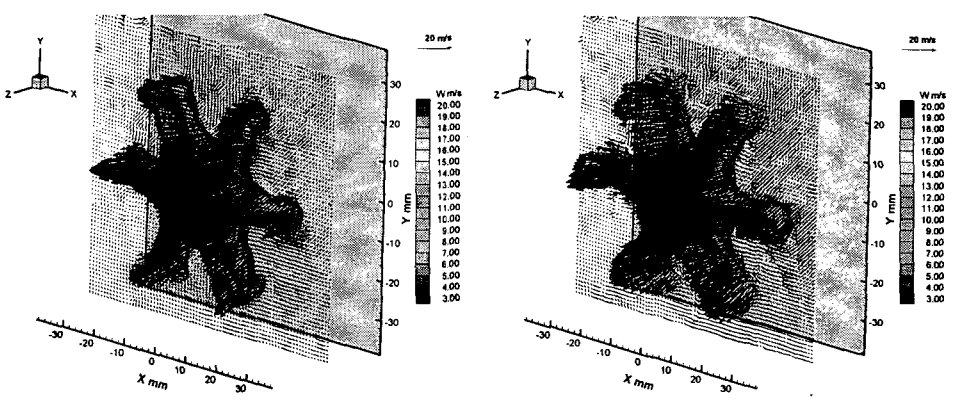

a. instantaneous velocity field in Z=10mm cross plane

b. simultaneous velocity field in Z=12mm cross plane

Fig. 3. A pair of typical instantaneous velocity fields obtained simultaneously by using the dual-plane stereoscopic PIV system

According to the definition of vorticity vector, the three components of the normalized vorticity vectors in the lobed jet mixing flow can be calculated by using following questions:

$$\varpi_x = \frac{D}{U_0}\left(\frac{\partial w}{\partial y} - \frac{\partial v}{\partial z}\right) \qquad (1)$$

$$\varpi_y = \frac{D}{U_0}\left(\frac{\partial u}{\partial z} - \frac{\partial w}{\partial x}\right) \qquad (2)$$

$$\varpi_z = \frac{D}{U_0}\left(\frac{\partial v}{\partial x} - \frac{\partial u}{\partial y}\right) \qquad (3)$$

Where D is the diameter of the lobed nozzle, and U_0 is the velocity of the jet flow at the test nozzle inlet. While, u, v and w are the instantaneous velocity in *X*, *Y* and *Z* directions (Fig. 2).

It should be noted that the terms like $\frac{\partial u}{\partial z}$ and $\frac{\partial v}{\partial z}$ in the above equations can not be determeined from the measurement result of a "classical" 2-D PIV system or a conventional "single-plane" stereoscopic PIV system. Therefore, only the out-of-plane componet of the vorticity ϖ_z with its direction normal to the illuminted laser plane can be obtained instantanously.

Since the present dual-plane stereoscopic PIV system can measure the velocity fields at two illuminated planes simultaneously, all the terms in the above vorticity definition equations can be calculated. Besides the out-of-plane component componet ϖ_z, the other two in-plane components of the vorticity vectors (ϖ_x and ϖ_y) can also be obtained in either of the two illuminated planes with first-order approximation and in the central plane between the two parallel illuminated planes with second-order approximation accuracy. By using the simultaneous measurement results of the dual-plane stereoscopic PIV system in Z=10mm and Z=12mm cross planes (Fig. 3), all the three components of the instantaneous vorticity vectors in the Z=10m cross plane were calculated. The results are shown in the Fig.4(a), 4(b) and 4(c).

As mentioned above, there are two kinds of vortices which are very important for the mixing process in lobed mixing flows: One is the large-scale streamwise vortices generated by the special geometry of lobed nozzle, another is the zaimuthal vortices rolled up at the interface of the shear layers due to the Kelvin-Helmholtz instability. For the large-scale streamwise vortices generated by the special trailing edge of the lobed nozzle, their existance were revealed very clearly from the instantaneous streamwise vorticity distribution shown in Fig. 4(c). In order to reveal the azimuthal vortices rolled up in the lobed mixing flows due to the Kelvin-Helmholtz instability, the x-component and y-component of the vorticity vectors were combined into in-plane vorticity by using the following equation:

$$\varpi_{in-plane} = \sqrt{\varpi_x^{\,2} + \varpi_y^{\,2}} \qquad (4)$$

Based on the equation (4), the distribution of the azimutha (in-plane) vorticity in the Z=10mm cross-plane of lobed jet mixing flow was calculated (Fig. 4(d)). As it is expected, the azimuthal Kelvin-Helmholtz vortex ring was found to have the same geometry as the lobed trailing edge at the exit of the lobed nozzle.

It should be noted that although the existances of the streamwise vortices and the azimuthal Kelvin-Helmholtz vortices in lobed mixing flow have been suggested in previous studies, the quantitative data about the distributions of streamwise vorticity and azimulthal vorticity in lobed mixing flows have never been obtained due to the limitation of the experimental techniques used in those previous studies. The measurement results obtained by the present dual-plane stereoscopic PIV system are likely to be the first to reveal the streamwise vortices and the azimuthal Kelvin-Helmholtz vortices in the lobed jet mixing flows instantaneously and simultaneously.

Based on the 200 frames of instantaneous measurement results, the ensemble-averaged streamwise vorticty and azimuthal (in-plane) vorticity distributions in the lobed jet mixing flow at Z=10mm cross plane were calculated, which are given in Fig. 4(e) and Fig. 4(f). Compared with the instantaneous streamwise and azimuthal vorticity fields, the ensemble-averaged streawise and azimuthal vorticity fields were found to be much smoother. However, they have almost the same distribution pattern and magnitude as their instantaneous counterparts, which indicate that the generation of the streamwise vortices and azimuthal vortex ring at the exit of the lobed nozzle are quite steady.

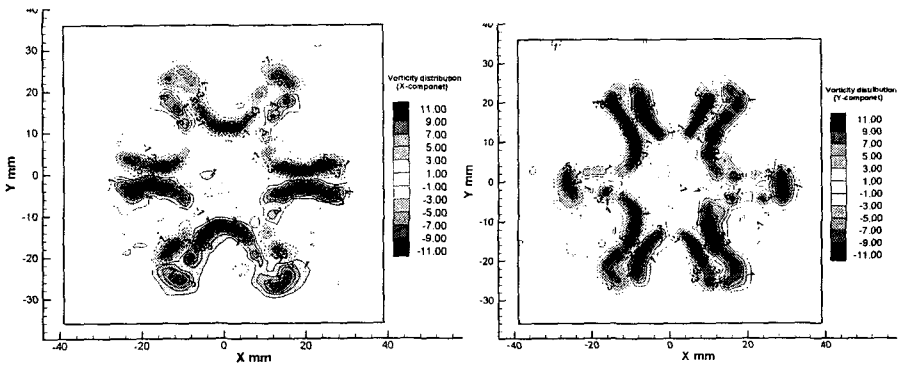

a. instnatanous vorticity (X-component)　　b. instnatanous vorticity (Y-component)

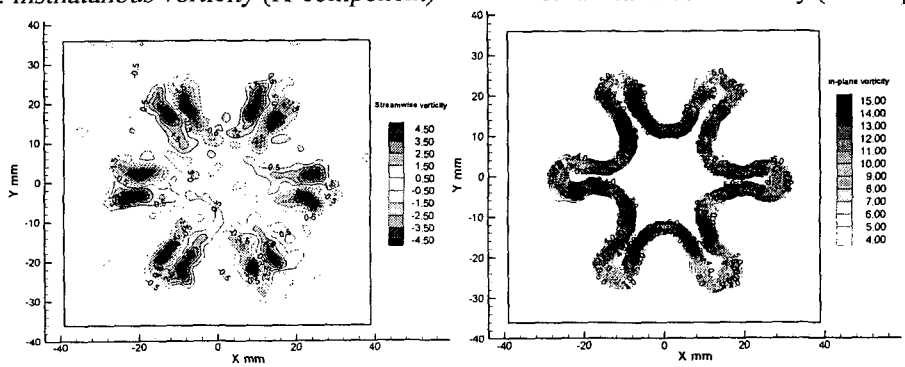

c. instantaneous streamwise vorticity (Z-component)distribution　　d. instantaneous azimuthal (in-plan)vorticity distribution

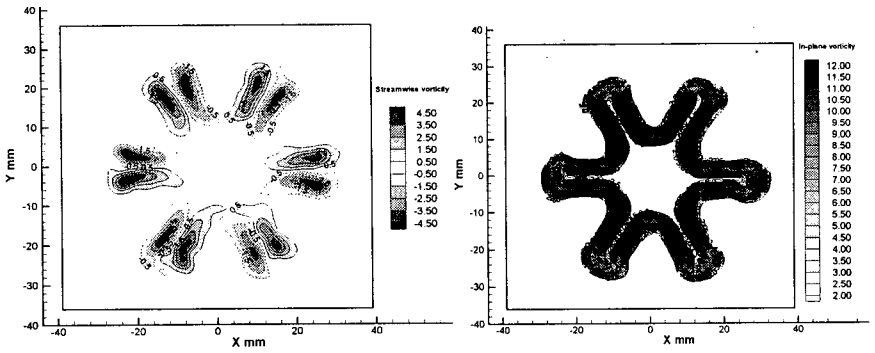

e. ensemble-averaged streamwise vorticity distribution

f. ensemble-averaged azimuthal (in-plane)vorticity distribution

Fig 4. The streamwise and azimuthal vorticity distributions in the Z=10mm cross plane of the lobed jet mixing flow

Figure 5 shows the simultaneous measurement results of the streamwise vorticity and azimuthal vorticity distributions in the Z=20mm (Z/D=0.5, Z/H=1.33) cross plane of the lobed jet mixing flow. The six pairs of counter-rotating streamwsie vortices generated by the lobed nozzle were found to be deformed in the instantaneous streamwise vorticity field. Some of the large-scale streamwise vortices were even found to begin to break into smaller vortices. Besides the six pairs of large-scale streamwise vortices corresponding to the six lobes, six pairs of smaller and weaker streamwise vortices at the six lobe troughs can also be identified from the instantaneous streamwise vorticity distributions. The large azimuthal vortex-ring with the same geometry as the trailing edge of the lobed nozzle can still be seen from the ensemble-averaged azimuthal vorticity distribution. However, the maximum magnitude of the ensemble-averaged azimuthal vorticity (11.0), is found to be a bit smaller than that of its instantaneous counterpart, which is about 15.0

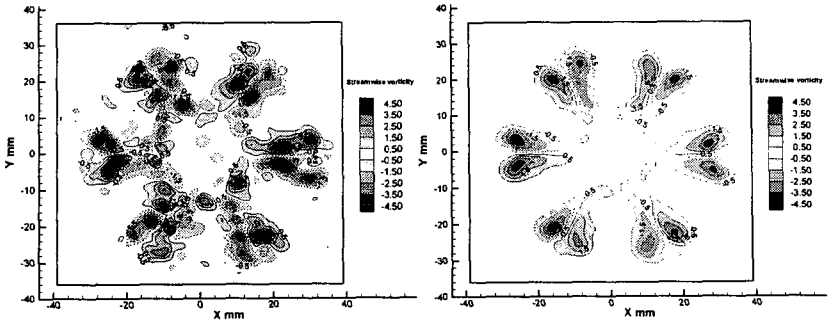

a. instantaneous streamwise vorticity distribution

b. ensemble-averaged streamwise vorticity distribution

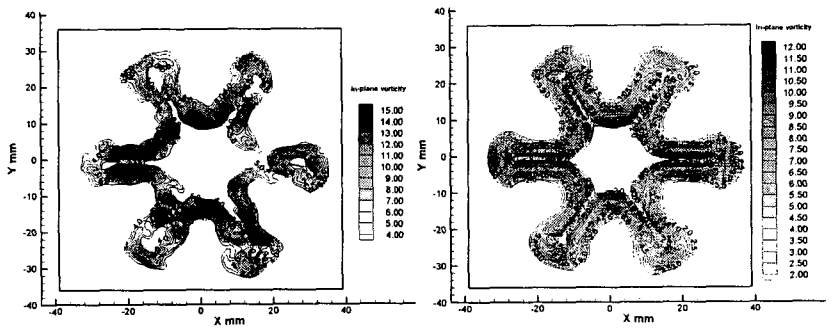

c.instaneous azimuthal vorticity distribution

d. ensemble-averaged azimuthal vorticity distribution

Fig. 5. The measurement results of the dual-plane stereoscopic PIV system at Z=20mm (Z/D=0.50, Z/H=1.33) cross plane

In the Z=40mm (Z/D=1.0, Z/H=2.67) cross plane, the six pairs of the large-scale streamwise vortices (Fig. 6(a)) were found to deform more seriously. More and more large-scale streamwise vortices were found to break into smaller vortices. The adjunct streamwise vortices were found to merge with each other to form a vortex ring structure in the lobe troughs. From the ensemble-averaged streamwise vorticity distributions shown on Fig. 6(b), the six pairs of large-scale streamwise vortices were found to grow and expand radially. The strength of these ensemble-averaged streamwise vortices were found to decrease quite much with the maximum value of the ensemble-averaged streamwise vorticity only about the half of that at the Z=10mm (Z/D=0.25, Z/H=0.67) cross plane.

From the instantaneous azimuthal vorticity distribution given in Fig. 6(c), it can be seen that the azimuthal vorticity ring, which has the same geometry as the lobed nozzle trailing edge at the exit of the lobed nozzle, has broken into many disconnected vortical tubes in this cross plane. The azimuthal tubes at the lobe troughs was found to begin to reconnect again to form a new circular-ring-like-structure in the center of the jet flow. Same phenomena have been revealed clearly form the planar LIF flow visualization images of the earlier work of the authors (Hu et al. 2000a,b).

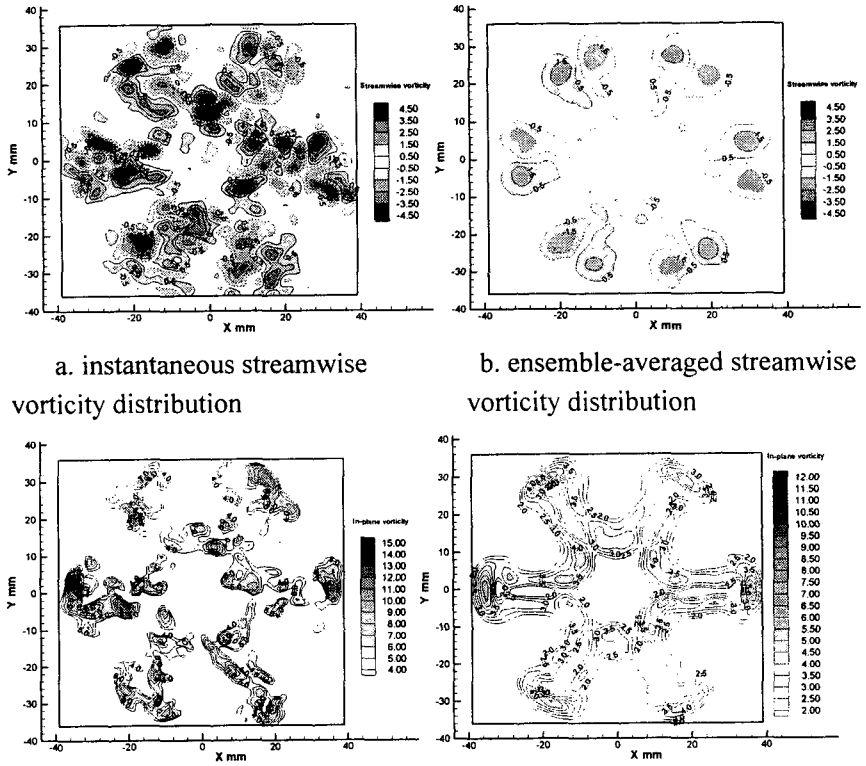

a. instantaneous streamwise vorticity distribution

b. ensemble-averaged streamwise vorticity distribution

c. instantaneous azimuthal vorticity distribution

d. ensemble-averaged azimuthal vorticity distribution

Fig. 6. The measurement results of the dual-plane stereoscopic PIV system at Z=40mm(Z/D=1.0, Z/H=2.67) cross plane

McCormick and Bennett (1994) suggested that the streamwise vortices deform the azimuthal Kelvin-Helmholtz vortical tube into pinch-off structures due to the interaction between the streamwise vortices and azimuthal Kelvin-Helmholtz vortices. Such pinched-off effect of the azimuthal vortex tubes can be seen very clear and quantitatively from the ensemble-averaged azimuthal vorticity distribution given in the Fig. 6(d). The cutting of the large azimuthal vortex ring and reconnecting of the azimuthal vortex tubes at the lobe troughs to form a new circular-ring-liked-structure in the center of the lobed jet flow can also be seen from the ensemble-averaged azimuthal vorticity distribution.

As the downstream distance increased to Z=60mm (Z/D=1.5, Z/H=4.00), the six pairs of large-scale streamwise vortices generated by the lobed nozzle could no longer be easily identified from the instantaneous streamwise vorticity field shown in Fig. 7(a). Instead of large-scale streamwise vortices, many smaller streamwise vortices were found in the flowfield. It means the large-scale streamwise vortices observed in the upstream cross planes have broken down into many smaller streamwise vortices. It should be mentioned that the maximum vorticity of these smaller streamwise vortices are found to be almost at the same level as their parent streamwise vortices in the upstream cross planes.

From the ensemble-averaged streamwise vorticity distribution shown in Fig. 7(b), it can be seen that the large-scale streamwise vortices revealed in the ensemble-averaged streamwise vorticity distributions of upstream cross planes were also found to break down into smaller vortices. The strength of these ensemble-averaged streamwise vortices decayed substantially, and the maximum value of the ensemble-averaged streamwise vorticity was found to be only about one fourth of that at Z=10mm (Z/D=0.25, Z/H=0.67) cross plane.

The azimuthal vortex ring, which has the same geometry as the lobed nozzle trailing edge at the nozzle exit, was found to break into many disconnected vortical tubes completely in this cross plane.

A new circular-ring-like-structure due to the reconnecting of the azimuthal vortex tubes at the lob troughs can be found in the center of the jet flow, which is similar to the circlar azimuthal vortex rin in a circular jet flow. The circular-ring-like-structure in the central of the jet flow can been seen mor clear from the ensemble-averaged azimuthal vorticity distribution, while the azimuthal vortex tube corresponding to the lobed peaks were found to form six "crescents" in this cross plane. Due to th intensive mixing between the core jet and ambient flow, the strength of the azimuthal vortices ha dissipated very much. The maximum value of the ensemble-averaged azimuthal vorticity was foun to be only about one fourth of that at the exit of the lobed nozzle.

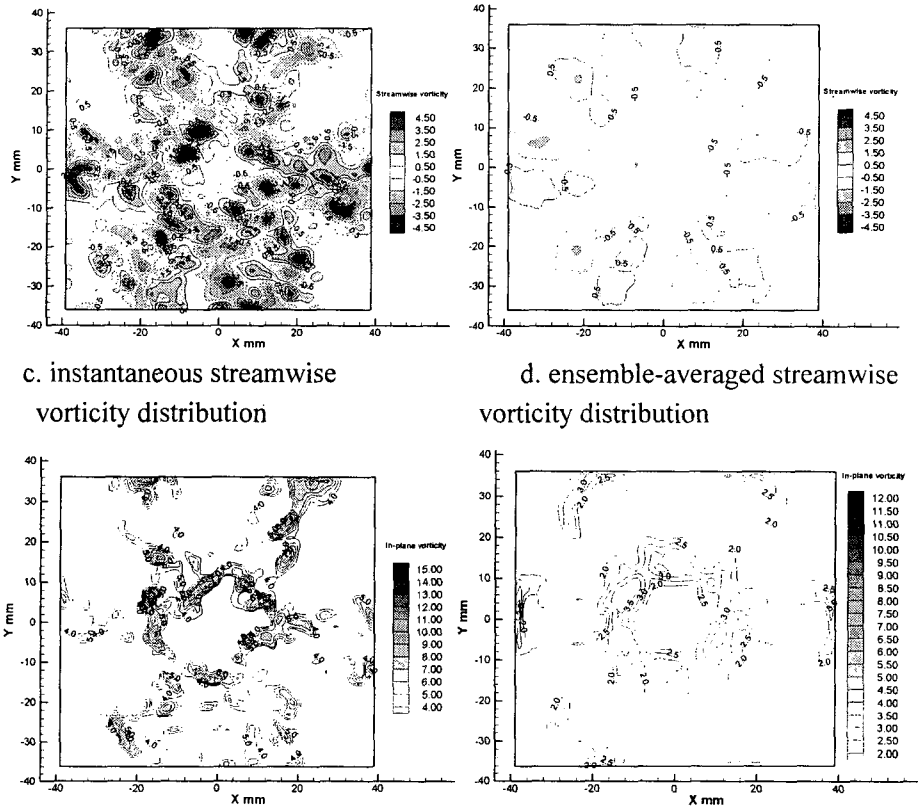

c. instantaneous streamwise vorticity distribution

d. ensemble-averaged streamwise vorticity distribution

e. instantaneous azimuthal vorticity distribution

f. ensemble-averaged azimuthal vorticity distribution

Fig. 7. The measurement results of the dual-plane stereoscopic PIV system at Z=60mm (Z/D=1.5, Z/H=4.0) cross plane

As the downstream distance increases to Z=80mm (Z/D=2.0, Z/H=5.33), the lobed jet mixin flow was found to be more and more turbulent. The smaller but not weaker streamwise vortice originated from the breakdown of the large-scale streamwise vorticity generated by the lobed nozzl almost fully filled the measurement window (Fig. 8 (a)). Since these small-scale streamwise vortice is so unsteady and they appear in the flow field very randomly, only very vague vortical structure can be identified from the ensemble-averaged streamwise vorticity distribution. Th ensemble-averaged streamwise vorticity distribution shown in Fig. 8(b) revealed that th ensemble-averaged streamwise vortices have been dissipated so seriously that their stength is onl about one tenth of that in Z=10mm upstream cross plane.

Due to the intensive mixing between the core jet flow and ambient flow, the azimuthal vortice also dissipated substantially. The six "crescents" formed by the azimuthal vortex tubes at the lobe peak regions almost disappeared in the flow field, and only the circular-ring-like-structure in th center of the jet flow can be identified from the ensemble-averaged azimuthal vorticity distributio with its strength dissipated substantially.

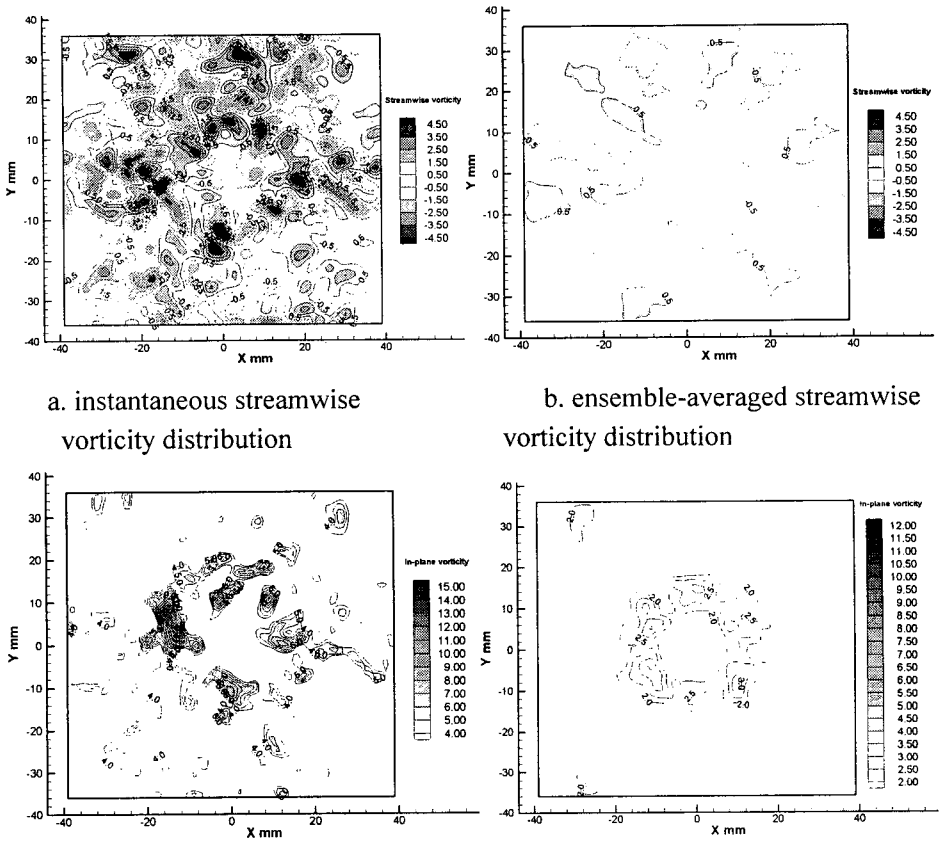

a. instantaneous streamwise vorticity distribution

b. ensemble-averaged streamwise vorticity distribution

c. instantaneous azimuthal vorticity distribution

d. ensemble-averaged azimuthal vorticity distribution

Fig. 8. The measurement results of the dual-plane stereoscopic PIV system at Z=80mm (Z/D=2.0, Z/H=5.33) cross plane

From the above instantaneous streamwise distributions in different downstream cross planes, it can be seen that as the downstream distance increases, the size of the instantaneous streamwise vortices in the lobed jet mixing flow became smaller and smaller. It means the large-scale streamwise vorticity generated by the lobed nozzle break into smaller vortices as they travel downstream. However, the maximum vorticity values of the smaller vortices were found to be almost at the same level as their parent streamwise vortices. These results suggest that the dissipation of the large-scale streamwise vortices generated by the corrugated trailing edge of the lobed nozzle did not happen abruptly, but rather appeared to be a gradual process. The large streamwise vortices were found to break down into many smaller, but not weaker streamwise vortices as the downstream distance increasing. Thus, besides the mixing enhancement at large scale, mixing at a finer scale could also be achieved in the lobed jet mixing flow. The result, therefore, agrees well with those obtained by Milam et al. (1997)

The ensemble-averaged streamwise vorticity distribution can be used to indicate the overall effect of the special geometry of the lobed nozzle on the mixing processes in the lobed jet mixing flows. The special geometry of the lobed nozzle results in the generation of large-scale ensemble-averaged streamwise vortices in the lobed jet mixing flow. The large-scale ensemble-averaged streamwise vortices revealed in the ensemble-averaged streamwise vorticity distributions were found to grow up and expand radially within the first diameter, which may correspond to the streamwise vortex formation and intensification steps suggested by Werle et. al. (1987)and Eckerle et al. (1990) (Their LDV measurement results only revealed the ensemble-averaged streamwise vortices in a planar lobed mixing flow). The large-scale ensemble-averaged streamwise vortices were found to break down into smaller vortices at further downstream regions. Figure 10 gives the decay of the maximum value of the ensemble-averaged streamwise vorticity in the lobed jet flow quantitatively.

From the figure, it can be seen that at the first diameter of the test nozzle, the ensemble-averaged streamwise vorticity decayed very rapidly. At downstream region of Z/D>1.0 (Z/D>2.67), the large-scale ensemble-averaged streamwise vortices were found to break down into many smaller vortices, then the decay rate of the ensemble-averaged streamwise vorticity slows down. Further downstream (Z/D>3.0, Z/H>8.0), the ensemble-averaged streamwise vorticity dissipated so seriously that the strength of the streamwise vortices became about one tenth of that at lobed nozzle exit. This may indicate that the overall effect of the special geometry of the lobed nozzle on the enhanced mixing process in the lobed jet flow has almost disappeared at this downstream location.

For the azimuthal vortices in the lobed jet mixing flow, they were generated at the interface of the mixing streams due to the Kelvin-Helmholtz instability existed at any shear layer. Therefore, the azimuthal vortex ring at the nozzle exit has the same geometry as the lobed nozzle trailing edge. Due to the interaction between the streamwise vortices, the azimuthal vortex ring deformed into pinched-off structures first, then broke down into disconnected substructures as they travel downstream. The broken azimuthal vortex tube pieces at the lobed troughs were found to reconnect with each other to form a new circular-ring-like-structure at the center of the lobed jet flow, while the azimuthal vortex tubes corresponding to the lobed peaks were found to form six "crescents" structures. The six "crescents" structures were found to dissipated out further downstream,, and only very indistinct circular-ring-like-structure can be found at the central of the jet mixing flow.

The decay of the maximum value of the ensemble-averaged azimuthal vorticity in the lobed jet mixing flow is also given in the Fig. 10. It should be noted that the decay profile of the azimuthal vorticity is very similar to that of the streamwise vorticity. The ensemble-averaged azimuthal vorticity decay very rapidly winthin the first one diameter of the lobe nozzle, then turns to be a more moderate rate further downstream. This may be explained by that within the first one diameter of the test nozzle (Z/D<1.0, Z/H<2.67), due to the stirring effect of the large-scale streamwise vortices revealed in the ensemble-averaged streamwise vorticity distributions, the core jet flow and ambient flow mixed intensively. The velocity of the core jet flow decays very rapidly. Weaker and weaker shear layer (lower velocity ratio) is expected in the lobed jet mixing flow as the downstream distance increases. Therefore, the magnitude of the azimuthal vorticty decays very quickly within the first diamter of the lobed nozzle. In the downstream region of 1.0<Z/D<2.0, the large-scale streamwise vortices were found to breake down into smaller vortices, the strength of large-scale streamwise vortices generated by the special geometry of the lobed nozzle were found to be dissipated very seriously, i.e, the stirring effect of the ensemble-averaged streamwise vortices weakened. The velocity decay of the core jet flow slows down, therefore, the decay rate of the azimuthal vorticity is also found to slow down. The ensemble-averaged streamwise vorticity dissipated

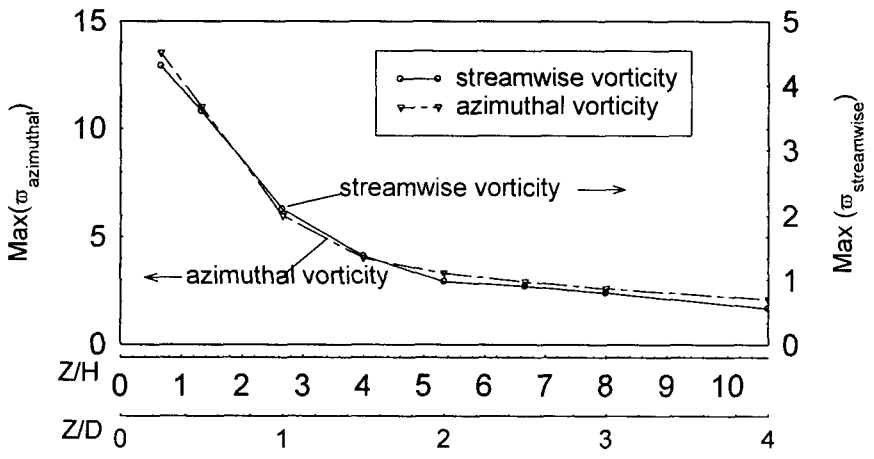

Fig.10. The decay of the ensemble-averaged streamwise vorticity and azimuthal vorticity in the lobed jet mixing flow

so seriously further downstream that they almost can not be indentified in the flow field anymore, and the enhancement mixing due to the stiring effect of large-scale streamwise vortices has be

finished, the mixing between the core jet flow and ambinet flow is expected to ocurr at the same gradient-type mechanism as that for a circular jet flow, therefore, the azimuthal vorticity decay very slowly and linearly as that in a circular jet flow.

4. Conclusions

In the present study, the streamwise vorticity and azimuthal vorticity distributions in a lobed jet mixing flow were measured simultaneously by using a novel dual-plane stereoscoipic PIV system. The evolution and interaction characteristics of various vortical structures in the lobed jet mixing flow were analyzed based on the simultaneous vorticity measurement results of the dula-plane stereoscoipic PIV system.

5. References

Belovich V. M. and Samimy M. (1997), Mixing Process in a Coaxial Geometry with a Central Lobed Mixing Nozzle. AIAA Journal Vol.35, No.5 PP838-841.

Eckerle W. A., Sheibani H. and Awad J., (1990), Experimental Measurement of Vortex Development Downstream of a Lobed Forced Mixer, ASME 90-GT-27.

Elliott G.S. and Beutner T. J. (1999), Molecular Filter Based Planar Doppler Velocimetry, Progree in Aerospace, vol. 35, pp799-845.

Elliott J.K, Manning T.A.,Qiu Y. J., Greitzer, C.S., Tan C.S. and Tillman T.G, (1992), Computational and Experimental Studies of Flow in Multi-Lobed Forced Mixers, AIAA paper 92-3568.

Hu H., Saga T., Kobayashi T., Taniguchi N., Liu H. and Wu S., (1999), Research on The Rectangular Lobed Exhaust Ejector/Mixer Systems, Transactions of Japan Society of Aeronautics and Space Science. Vol.41 No.134, pp187-194.

Hu H., Kobayashi T., Saga T. and Taniguchi N. (2000a) PIV and LIF Measurements on the Lobed Jet Mixing Flows, Experiments in Fluids Vol.29, No.7, pps141-157.

Hu H., Saga T. and Kobayashi T. (2000b) Research on the Vortical and Turbulent Structures in the Lobed Jet Flow by Using LIF and PIV ", Measurement Science and Technology, Vol.11, pp698-711

Hu H., Saga T., Kobayashi T., Taniguchi N. and Segawa S., (2000c) The Spatial Resolution Improvement of PIV Result by Using Hierarchical Recursive Operation, Proceedings of 9th International Symposium on Flow Visualization, Edinburgh, Scotland, UK, Aug. 22-25. 2000.

Hu H., Saga T., Kobayashi T. and Taniguchi N. (2001a) A Study on a Lobed Jet Mixing Flow by Using Stereoscopic PIV Technique, Physics of Fluids (accepted)

Hu H., Saga T., Kobayashi T., Taniguchi N. and Yasuki M. (2001b), Dual-plane Stereoscopic PIV: System Setup and Its Application on a Lobed Jet Mixing Flow, Experiments in Fluids (accepted, in press)

Kaehler C. J. and Kompenhans J. (1999), Multiple Plane Stereo PIV: Technical Realization and Fluid-Mechanical Significance, Proceedings of The 3rd International Workshop on PIV, Santa Barbara, U.S.A, Sep.16-18, 1999.

Kaehler C. J. (2000), Multiple Stereo PIV- recording and evaluation methods, Proceedings of EUROMECH 411, Rouen, France, May 29-31, 2000.

Kuchar, A. P. and Chamberlin, R., (1980) Scale Model Performance Test Investigation of Exhaust System Mixers for an Energy Efficient Engine (E^3)", AIAA paper 80-0229.

Melling A. (1997), Tracer Particles and Seeding for Particle image Velocimetry, Measurement Science and Technology, Vol.8, pp1406-1416.

McCartney E. (1976), Optics of the atmosphere: scattering by molecules and particles, Now York: Wiley.

McCormick D.C. and Bennett J.C.Jr. (l994) Vortical and Turbulent Structure of a Lobed Mixer Free Shear Layer" AIAA Journal, Vol.32, No.9. pp1852-1859.

Milam, D.M., Samimy M., and Martens, S., 1997, A Study of Lobed-Mixer Using Simultaneous LIF and Mie Scattering," Journal of Propulsion and Power, Vol. 13, No.3, pp.445-448.

Paterson R. W., (1984) Turbofan Forced Mixer Nozzle Flowfield- A Benchmark Experimental Study, ASME Journal of Engineering for Gas Turbines and Power Vol.106, pp692.

Prasad A. K. and Jensen K, (1995), Scheimpflug Stereocamera for Particle Image Velocimetry in Liquid Flows, Applied Optics, Vol.34, 7092-7099

Prasad A. K. (2000), Stereoscopic Particle Image Velocimetry, Experiments in Flows, Vol. 29 pp103-116

Presz, Jr. W. M., Reynolds, G. and McCormick, D., (1994), Thrust Augmentation Using Mixer-Ejector-Diffuser Systems. AIAA Paper 94-0020.

Smith L.L, Majamak A.J., Lam I.T. Delabroy O.,Karagozian A.R., Marble F.E. and Smith, O. I., (l997) Mixing Enhancement in a Lobed Injector. Phys. Fluids, Vol.9 No.3 pp667-678

Soloff S. M., Adrian R. J. and Liu Z. C. (1997), Distortion Compensation for Generalized Stereoscopic Particle Image Velocimetry, Measurement Science and Technology, Vol.8 pp1441-1454.

Werle M.J., Paterson R. W. and Presz Jr. W. M., (1987) Flow Structure in a Periodic Axial Vortex Array, AIAA paper 87-6l0.

Willert C. (1997), Stereoscopic Digital Particle Image Velocimetry for Application in Wind Tunnel Flows. Measurement Science and Technology, Vol.8 pp1465-1479.